Characterization of conductive particles dispersion in textile coatings through Joule's effect monitoring analysis

RUIZ-CALLEJA Tamara[1], JIMÉNEZ-SUÁREZ Alberto[1], CALDERÓN-VILLAJOS Rocío[1], PROLONGO Silvia G[1,2]

[1]Universidad Rey Juan Carlos, Calle Tulipán, 28933 Móstoles, Spain

[2] Instituto de Tecnologías para la Sostenibilidad. Universidad Rey Juan Carlos.

Corresponding author: Jiménez-Suárez, Alberto. Calle Tulipán, 28933 Móstoles, Spain. E-mail: alberto.jimenez.suarez@urjc.es

Abstract

Achieving proper dispersion of pigments, dyes, or other additives, such as microcapsules or nanoparticles, within printing pastes or textile coatings is crucial for obtaining a homogeneous result. In certain specialized applications, such as coloration technology, it is possible to use colorimetry tools, visual examination, and even artificial vision to identify defects. However, none of these techniques comprehensively map the specific additive distribution. This paper proposes a novel approach: monitoring the distribution of conductive particles (graphene nanoplatelets, referred to as GNP) within an acrylic coating paste using Joule's effect. Four different dispersion systems (ultrasound mixer, blender, toroidal agitation, and three-roll mill) are employed. Thermographic images provide an accurate view of how conductive particles are distributed. This complements data from numerical values like maximum and average temperatures recorded for each sample. In certain cases, relying solely on numerical values can be inadequate or insufficient, hence the novelty of this article emphasizing the significance of using Joule's effect to assess the distribution of conductive particles. Concerning the mixing systems, optimal dispersion of GNP in distilled water is most effectively achieved using an ultrasound mixer, with enhanced uniformity as dispersion time increases. For mixing the components of the coating paste, the toroidal agitation method yields the best result. Employing the three-roll mill is discouraged for this application due to its propensity to induce phase separation.

Keywords: graphene, coating, textile, conductive, Joule's heating

1. Introduction

The range of elements that can be incorporated into textile coatings is practically limitless, offering a wide array of applications for fabrics[1,2]. These include dyes and

pigments for adding color to textile surfaces[3–5], microcapsules that can hold aromas or medicines[6–9], additives for photoprotection[10] or self-cleaning, and nanoparticles[11,12] with properties like antimicrobial or electrical conductivity, such as silver or carbon-based structures[13–16] like graphene, nanotubes, and fullerenes. This demonstrates the diverse and versatile nature of the textile industry.

Numerous techniques are available for applying additives to functionalize textiles. Joshi et al.[17] present the following breakdown: fluid coating (such as paste or solution) can be employed via techniques like knife coaters, roll coaters, impregnators, and spray coaters. Meanwhile, solid coating materials (like powder or film) can be applied to textiles using approaches such as melt coating, calandering, or lamination. The choice of coating technique hinges on factors such as the substrate's characteristics, polymer type, solution viscosity, and the desired end product.

In the textile industry, multiple dispersion systems are available, and the selection of a particular system is primarily influenced by the type of additive, solution composition, and viscosity. Among the commonly utilized equipment in laboratories, the magnetic stirrer[18] stands out. It employs magnetic bars inside the solution, which vary in size, and a magnet or set of magnets to induce rotation and facilitate mixing. However, its effectiveness diminishes when dealing with solutions of high viscosity. Ultrasonic dispersion consists of generating shock waves by collapsing cavitations, which then leads to collisions among particles, splitting and dispersing them[19,20]. Additionally, there are rotary mechanical mixers equipped with heads of various geometries, capable of achieving high rotational speeds and generating, shear forces, axial forces, or suction to obtain uniform dispersion[21,22]. The bead mill is another option, described as a milling chamber filled with petite ceramic beads and a milling rotor powered by a motor[23]. Lastly, the roller mills, boasting a configuration similar to calanders, exert shear force to blend components within solutions of high viscosity[24–26].

Multiple tests are available for identifying defects in textile coatings, employing either visual examination or mechanical assessments[27–29]. Instruments like a colorimeter can detect disparities in color within a coating containing pigments or coloring additives[30]. Similarly, artificial vision tools can detect imperfections on textile surfaces[31–33]. However, it is worth noting that none of these methods can offer insights into the precise distribution of particles within the coating. In this work, we propose an innovative and effective monitoring technique based on Joule’s effect, which is limited to analysis of the conductive particle distribution.

Joule’s effect determines that it is possible to heat a conductive material by applying an electric current as a consequence of the interaction between the charge carriers, electrons, and the body of the material[34]. Joule’s effect heating system requires the presence of conductive particles, at least, to reach the electrical percolation threshold level[35]. The composition of the conductive particles can be very

diverse; in addition to GNP, some studies use carbon nanotubes[36], and silver nanoparticles[37], or include a thin electroconductive layer using physical vapor deposition techniques[38,39]. This technique is used to heat different elements, including fabrics[40]. Previous investigations determine this method can be useful to detect defects, both manufacturing and wear-produced, in composite materials[41,42] and in conductive textile coatings, where it is recommended to apply a high voltage and low exposure time to identify the particle dispersion in the thermographic images[43].

This study has a double objective: on the one hand, it evaluates four distinct dispersion systems (ultrasound, blender, dispermat, and three-roll mill) to determine the most effective approach for achieving optimal dispersion of graphene nanoplatelets within an acrylic coating paste. To ensure an accurate comparison, all parameters are identical, including fabric composition and structure, GNP concentration, coating thickness, paste composition, and analyzed area. The only variations among the samples are the dispersion methods used in each case. On the other hand, it corroborates the significance of analyzing particle dispersion via Joule's effect, since the simple analysis of the temperatures reached by the different coatings is insufficient to determine the suitability of each one of them. Therefore, the novelty of this work resides in the analysis of the different dispersion methods and processing times to find the most optimal combination in conjunction with the thermographic analysis of the samples, since this information is decisive for the evaluation of the results.

2. Experimental

2.1. Materials

The fabric used for this research is a 50% cotton-50% flax twill with a mass per unit area of 210 g/m^2, a thickness of 0.55 mm, and chemically bleached in an industrial process. Before applying the coating paste, the fabric is ironed at 180 ºC to ensure surface homogeneity. The base coating paste is obtained using acrylic binder, acrylic thickener, deaerating agent, and ammonia 28%. Graphene nanoplatelets with an average size of 30 x 40 µm and 10 nm of thickness, synthesized by a modified Hummers method using flake graphite powders as the starting material, are supplied by Innovatec SC, S.L.

2.2. Coating paste dispersion procedure

Each coating paste contains 30 g/kg of thickener, 15 g/kg of acrylic binder, 10 g/kg of ammonia, 10 g/kg of GNP, 2 g/kg of deaerating agent, and distilled water up to 1 kg of solution.

To analyze the dispersion of the conductive particles, four types of dispersers are used:

- Ultrasound mixer: UP400S from Hielscher with a power of 400 W, setting a cycle of 0.5 s and the amplitude at 50 %.
- Blender: electromechanical mixer with a power of 1000 W.
- High-speed toroidal agitation: Dispermat AE model, provided by Lumaquin.
- Three-roll mill: Model 80E from Exakt Technologies with a gap of 15 and 5 µm for the first and second gap, respectively at a speed of 250 rpm for the first roll.

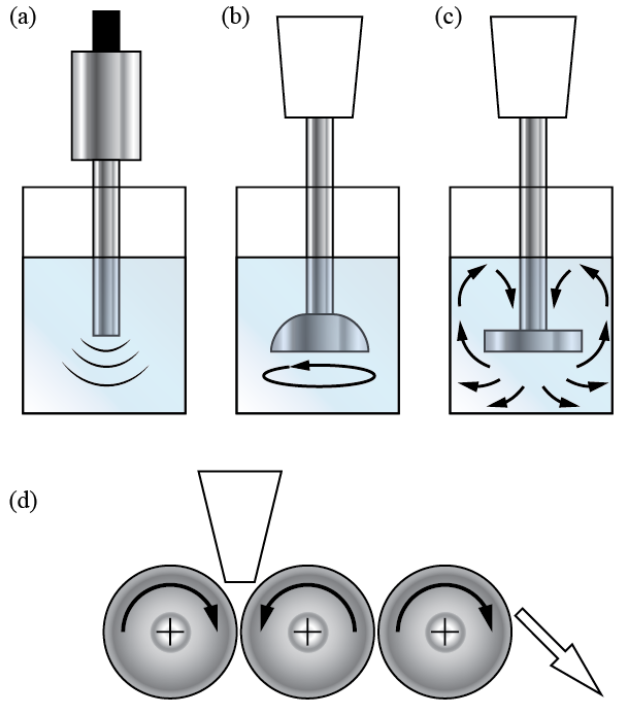

Figure 1. Schematic representation of (a) Ultrasound mixer; (b) Blender; (c) High-speed toroidal agitation; (d) Three-roll mill

The process of mixing the coating paste is conducted in two phases. Firstly, the dispersion of GNP in distilled water is carried out to achieve the most uniform distribution of conductive particles. Secondly, the remaining components of the coating paste are added to the aforementioned mixture. The nomenclature of the studied sample is collected in Table 1 considering the type of disperser and the processing time. The choice of parameters is based on findings from prior studies.

Table 1. Samples nomenclature and dispersion process information

GNP dispersion in water		Paste mixing		Nomenclature
Type of disperser	t [min]	Type of disperser	t [min]	
Ultrasound	5	Ultrasound	5	5U5U
Ultrasound	15	Ultrasound	5	15U5U

Ultrasound	30	Ultrasound	5	30U5U
Ultrasound	45	Ultrasound	5	45U5U
Ultrasound	5	Blender	5	5U5B
Ultrasound	15	Blender	5	15U5B
Ultrasound	5	Dispermat	5	5U5D
Ultrasound	15	Dispermat	5	15U5D
Ultrasound	5	Three-roll mill	2*	5U2C
Ultrasound	15	Three-roll mill	2*	15U2C
* This value indicates the number of three-roll mill cycles, not the time				

2.3. Fabric coating procedure

Fabric samples with a size of 20 x 30 cm are coated through a knife-coating technique, using both a metallic surface and a blade. The samples are fixed to the frame with a pressure grip. The blade is positioned at an angle of 90º and a gap of 1 mm from the surface. The coating paste is poured onto the fabric immediately following the dispersion process explained in section 2.2, then the coating paste excess is removed. The samples are oven-dried at 100 °C for 1 hour and, afterward, cured at 150 ºC for 3 minutes. When samples are dried, coating weight is reduced up to 95% due to moisture release, resulting in a dried coating weight of 62.5 ± 5% g/m^2. Figure 2 shows a schematic representation of the coating process described above.

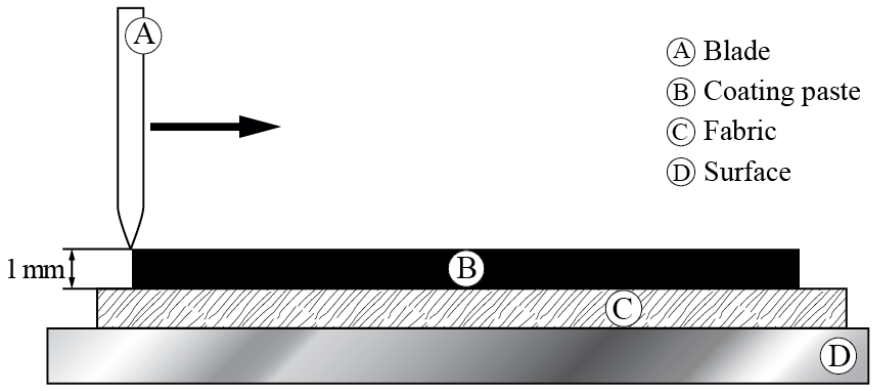

Figure 2. Schematic representation of the knife-coating process

2.4. Samples characterization

GNP dispersion in fresh samples of coating paste for 5U5U, 15U5U, 30U5U, and 45U5U is analyzed by light transmitted optical microscopy (TOM) in uncured dispersed resins, using a Leica DMR Optical Microscope equipped with a digital camera to take pictures. The GNP dispersion is measured using the software *ImageJ* to analyze the digital images. The microscopic observation of the samples is carried

out using a Field Emission Scanning Electron Microscope (FESEM) (ULTRA 55, ZEISS), with an acceleration voltage of 2 kV.

2.5. Coating evaluation through Joule's effect

Coated fabric samples are cut down to 4 x 10 cm, and copper wires are attached using silver paint to both ends distanced 8 cm, as depicted in Through Joule's effect, the thermoelectrical behavior of the samples is evaluated at 50 V using a programmable DC source-meter supply from Chroma. The thermal heating of each sample is recorded with an infrared thermal camera, model FlIR E50, placed 20 cm above the sample at an angle of 90º. Two samples of each coating are examined. During heating, thermographic images of the samples are captured after 0.5 s and the maximum and average temperatures are recorded after 60 s. Room temperature remains constant at 25 ºC.

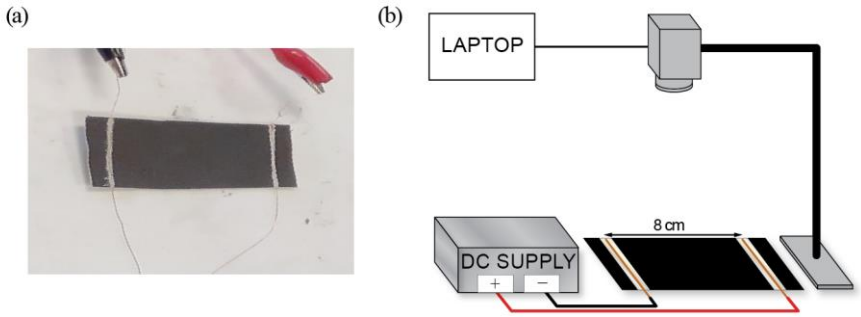

Figure 3. (a) Coated sample and (b) Joule's effect schematic setup

3. Results and discussion

3.1. Sample characterization

Figure 4 presents microscopic images taken of fresh coating paste from samples 5U5U, 15U5U, 30U5U, and 45U5U. These images depict that, as the mixing duration of GNP in water increases, the particle clusters disperse more uniformly. As calculated using ImageJ, the GNP dispersion in Figure 4.a, corresponding to 5U5U, amounts to 18.6% of the total image area. By extending the dispersion time of GNP in water to 15 minutes, as demonstrated in Figure 4.b for the 15U5U sample, the computed area increases to 31.0%. Regarding the samples subjected to 30 and 45 minutes of dispersion, the GNP-occupied area is found to be 38.5% and 45.2%, respectively. Repeating the measurements consistently confirmed that the margin of error is less than 0.1%. These measurements confirm a direct correlation: an extended GNP dispersion time in water corresponds to an enhanced homogeneity in particle distribution within the coating. After 45 minutes, no significant improvement in particle distribution is observed.

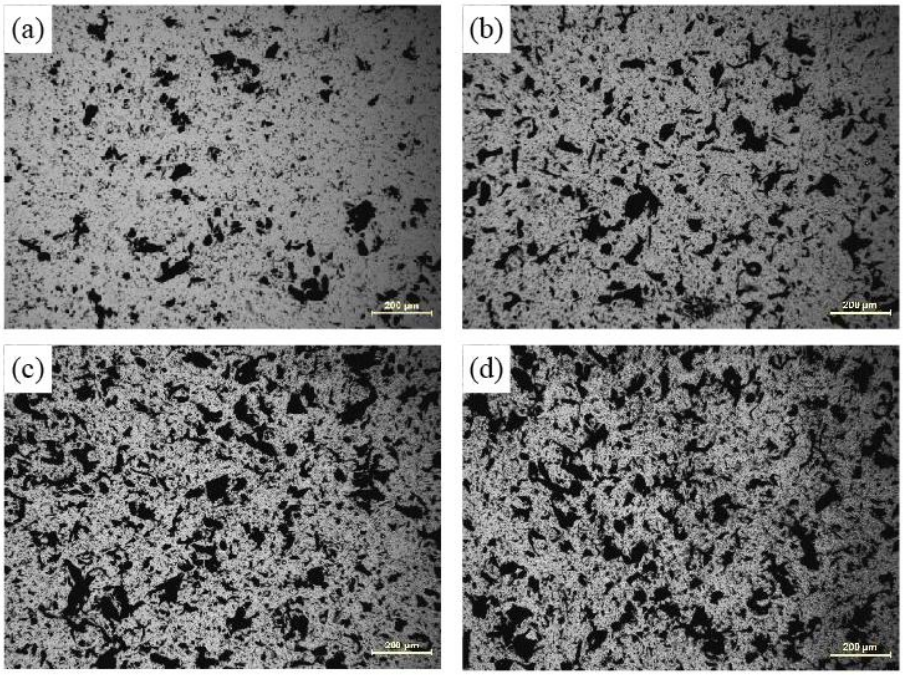

Figure 4. GNP dispersion analysis of fresh coating paste from samples (a) 5U5U, (b) 15U5U, (c) 30U5U, and (d) 45U5U.

3.2. Coating evaluation through Joule's effect

3.2.a. Thermographic images

The thermographic images from Figure 5 to Figure 8 depict the thermal changes observed in the samples after applying 50 V for 0.5 seconds. For enhanced comprehension of the conducted study, the images of the samples have been organized into a grid. The cells are arranged horizontally from 1 to 3 and vertically from A to D. Resulting from the Joule's effect, and facilitated by the utilization of FlIR software, these images provide a clear observation of the distribution pattern exhibited by the conductive graphene nanoparticles (GNP). The dispersion tendencies of these GNP particles are intricately linked to the specific type of disperser employed and the duration of the mixing process. A detailed analysis of each sample is presented below.

In the thermographic analysis of samples dispersed with ultrasound sonication, it can be observed that there is a certain heterogeneity in the coating. This is particularly noticeable in samples 5U5U (Figure 5.a), where a lack of conductive particles is found in cells B2 and C2, and 45U5U (Figure 5.d), where cells D1, D2, and C2 seem to have less GNP. While the preceding Section 3.1 corroborated a direct relationship between the duration of GNP dispersion in water through ultrasonic treatment and the resulting homogeneity of distribution, previous studies demonstrate the introduction of additional constituents within the coating paste induces significant alterations in the rheological properties of the paste. Consequently, despite the effective mixing achieved through ultrasound, obtaining an optimal integration of all components in the coating paste becomes technically complex when using an ultrasound disperser.

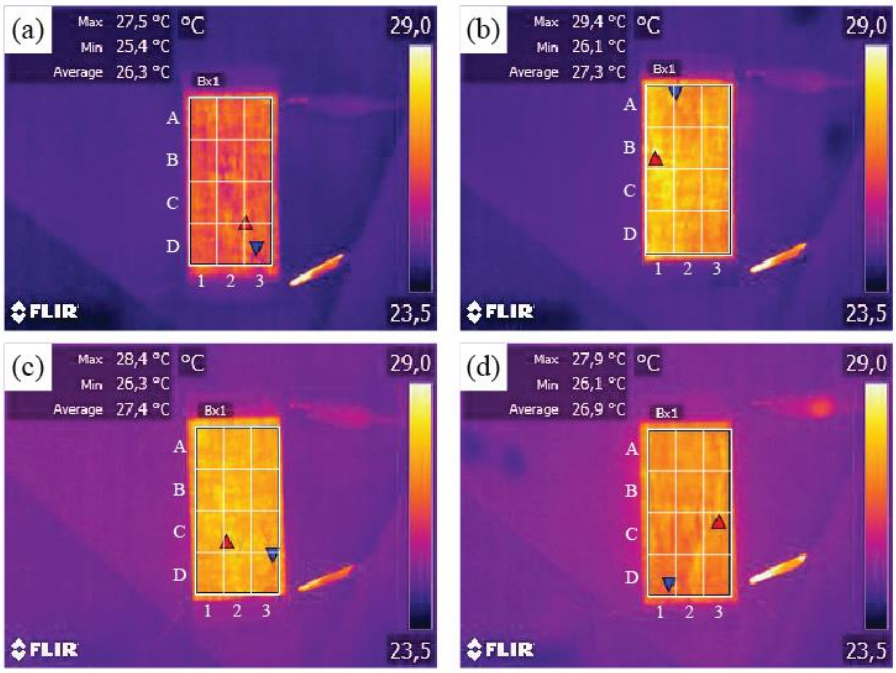

Figure 5. Thermographic images of samples (a) 5U5U, (b) 15U5U, (c) 30U5U, and (d) 45U5U.

Regarding the samples manufactured using ultrasound and a blender, Figure 6.a and Figure 6.b reveal a homogeneous temperature distribution. However, certain regions still exhibit noticeable differences in the concentration of conductive particles, as seen in cells A2 and C1-C2 for 5U5B and cells A1-A2 for 15U5B. The utilization of both ultrasound and a blender for dispersion produces satisfactory outcomes in terms of achieving a uniform distribution of conductive particles. A better result might have been achieved by extending the GNP dispersion time in water, as discussed in section 3.1. The chosen blender is appropriate to handle viscosities similar to that of the coating paste, however, it is important to mention that the blender's rotational speed capability is not as high as the dispermat, which could impact how evenly the mixture is blended.

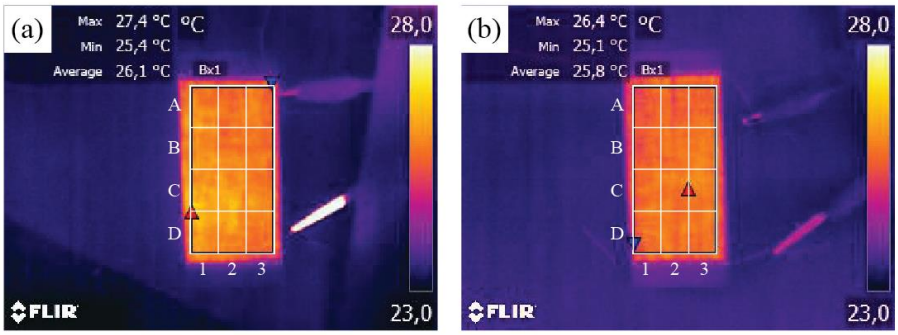

Figure 6. Thermographic images of samples (a) 5U5B and (b) 15U5B.

The samples developed using the dispermat method, seen in Figure 7.a and 7.b, show the highest regularity in the distribution of GNP. The presence of particle clusters or regions lacking particles is minimal, and the heating pattern is consistently

even across the entire surface of the samples for both 5U5D and 15U5D. This method stands out among the four examined. As commented in section 3.1, the results could be even better by letting the GNP disperse in water for longer. It is even worth considering executing both dispersion phases with the dispermat equipment.

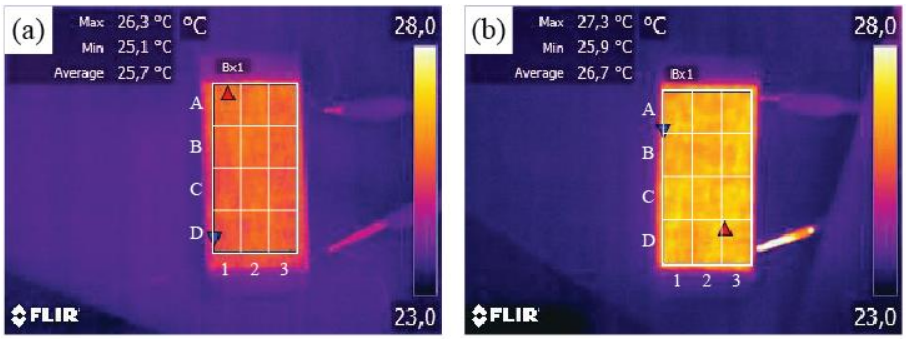

Figure 7. Thermographic image of samples (a) 5U5D and (b) 15U5D.

The samples produced by blending the coating paste ingredients using a three-roll mill exhibit a clear heterogeneous outcome, with highly differentiated areas where GNP accumulates (cells D1, B1, and C3 for 5U2C and column 3 for 15U2C) and other areas where it appears to be lacking (cells A1 to A3 and D3 for 5U2C and columns 1 a 2 for 15U2C). While making these samples, there was clear separation among the coating paste components, a phenomenon attributed to the shear force generated by this equipment. Additionally, a visual inspection of the sample, as seen in Figure 9, already suggested an uneven dispersion before the thermographic analysis, a similar phenomenon is described in scientific literature[44]. SEM images of the coating also confirm the heterogeneous particle distribution, while demonstrating a similar coating thickness on the surface of the fabric. Undoubtedly, the utilization of a three-roll mill is discouraged for this intended application.

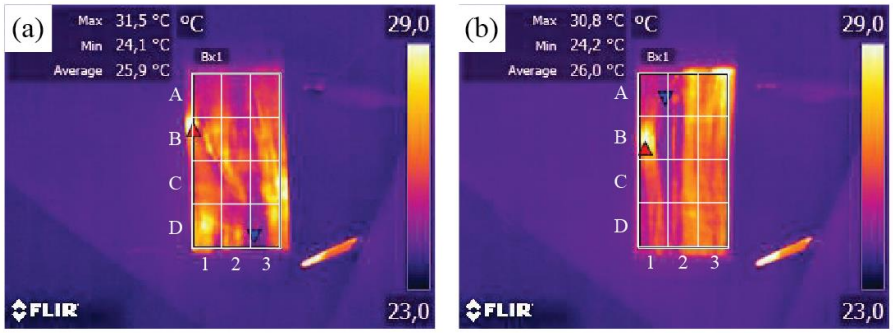

Figure 8. Thermographic images of samples (a) 5U2C and (b) 15U2C.

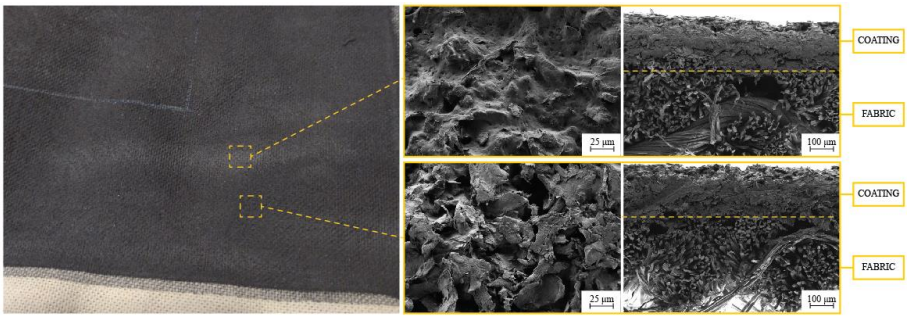

Figure 9. Image of the textile substrate coated with 5U2C and SEM images of the marked areas.

3.2.b. Mean and maximum temperature

The examination of average and maximum temperatures achieved by the samples after one minute of heating is particularly interesting. At first glance, it appears to suggest that the best heating results are from samples manufactured using the three-roll mill in the second phase of coating paste dispersion. However, a comprehensive assessment requires comparing these results with the corresponding thermographic images. This uniqueness underscores the novelty of this article and highlights the significance of using Joule's effect to evaluate conductive particle distribution. Additionally, it should be noted that by applying only 50 V, the samples reach high temperatures. Hence, with a reduced voltage, adequate temperatures can be achieved for the use of these fabrics in thermal comfort applications.

For samples 5U2C and 15U2C, the recorded average and maximum temperatures are notably high. This is attributed to localized regions with high GNP concentrations, as seen in Figure 8, juxtaposed with areas with hardly any GNP. While the numerical outcomes seem acceptable, the actual coating of these samples is not adequate. Furthermore, both of them obtain similar values. The three-roll mill is an effective dispersion method and, therefore, the dispersion achieved with ultrasound should not worsen it, hence the areas with higher concentration and good dispersion, understood as partial exfoliation of the GNP, conduct well. However, this equipment does not achieve good distribution and homogenization when adding the other components of the coating paste due to a significant change in the rheology.

Another aspect to consider is the difference between average and maximum temperatures in each sample. Samples with minimal temperature variation between both values likely show a more even coating, consistent with thermographic observations, which is the case of samples 5U5U, 45U5U, 5U5B, 5U5D, and 15U5D.

Similarly, the outcome obtained from samples 5U5D and 15U5D is quite remarkable. Despite being the samples with the most homogeneous dispersion, they surprisingly register the lowest average temperatures among all the samples subjected to examination. This phenomenon could be caused by the lack of areas with high GNP concentration, that increase the average temperature artificially. It is also worth

mentioning the relatively small standard deviation value observed among the samples analyzed for 5U5D and 15U5D, which states the excellent uniformity exhibited by the coatings dispersed with this method.

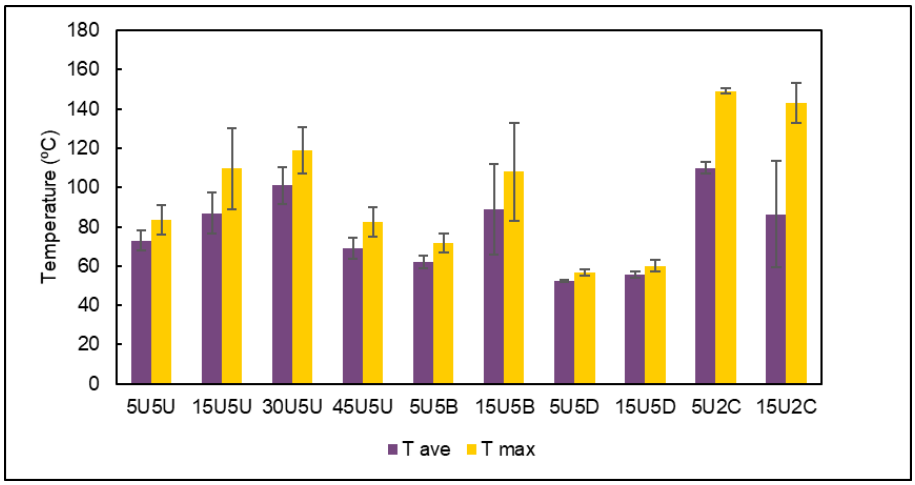

Figure 10. Average and maximum temperatures achieved by each sample at 50 V for 60 s.

4. Conclusions

Joule's effect, with slight heating up to 25-30ºC, has proven efficient in detecting the homogeneity of the samples and the presence of defects. This system has made it possible to verify that although the dispersion achieved is better the longer the sonication time, during the secondary addition stage a system is required that is particularly effective in the homogenization of the components and distribution of the nanoreinforcement within the mixing, which is achieved with high-speed stirring and toroidal energy.

Therefore, to obtain coatings on fabrics, it is considered that thermography can be a fast, efficient, and low-cost technique to assess whether the applied coatings have adequate characteristics on textile garments with minimal heating and consumption.

As a prospective line of research, it is suggested to explore coating non-conductive additives with methods such as spray or chemical vapor deposition to provide them with electrical conductivity. This approach would enable the assessment of particle dispersion via Joule's effect of non-conductive additives, thereby broadening the analytical possibilities in the textile field.

References

1. Shabbir M, Ahmed S and Sheikh JN. *Frontiers of Textile Materials: Polymers, Nanomaterials, Enzymes, and Advanced Modification Techniques*: John Wiley & Sons, 2020, p.62.

2. Darbra RM, Dan JG, Casal J, et al. Additives in the textile industry. In: Anonymous *Global Risk-Based Management of Chemical Additives I: Production, Usage and Environmental Occurrence*: Springer, 2012, p.83.

3. Riaz S, Ashraf M, Hussain T, et al. Functional finishing and coloration of textiles with nanomaterials. *Color Technol* 2018; 134(5): 327–346.

4. Huang M, Lu S-, Ren Y, et al. Structural coloration and its application to textiles: a review. *Text Inst* 2020; 111(5): 756–764.

5. Uddin MA, Rahman MM, Haque ANMA, et al. Textile colouration with natural colourants: A review. *J Clean Prod* 2022; 349: 131489.

6. Sousa VI, Parente JF, Marques JF, et al. Microencapsulation of Essential Oils: A Review. *Polymers* 2022; 14(9): 1730.

7. Singh N and Sheikha J. Microencapsulation and its application in production of functional textiles. *Indian J Fibre Text Res* 2020; 45: 495–509.

8. Oliveira JR, Guimarães VHD, Pereira UA, et al. The Use of Textiles in the Wound Healing: A Review. *Mini-Rev Med Chem* 2022; 22(10): 1438–1449.

9. Ghayempour S and Montazer M. Micro/nanoencapsulation of essential oils and fragrances: Focus on perfumed, antimicrobial, mosquito-repellent and medical textiles. *J Microencapsul* 2016; 33(6): 497–510.

10. Mondal S. Nanomaterials for UV protective textiles. *J Ind Text* 2022; 51(4_suppl): 5592S–5621S.

11. Rivero PJ, Urrutia A, Goicoechea J, et al. Nanomaterials for Functional Textiles and Fibers | Discover Nano. *Nanoscale Res Lett* 2015; 10: 1–22.

12. Jadoun S, Verma A and Arif R. Modification of textiles via nanomaterials and their applications. In: Anonymous *Frontiers of textile materials: polymers, nanomaterials, enzymes, and advanced modification techniques*: Wiley Online Library, 2020, p.135.

13. Nguyen Bich H and Nguyen Van H. Promising applications of graphene and graphene-based nanostructures. *Adv Nat Sci: Nanosci Nanotechnol* 2016; 7(2): 023002.

14. Karim N, Afroj S, Tan S, et al. Scalable Production of Graphene-Based Wearable E-Textiles. *ACS Nano* 2017; 11(12): 12266–12275.

15. Yang Z, Pang Y, Han X-, et al. Graphene Textile Strain Sensor with Negative Resistance Variation for Human Motion Detection. *ACS Nano* 2018; 12(9): 9134–9141.

16. Pu X, Li L, Liu M, et al. Wearable Self-Charging Power Textile Based on Flexible Yarn Supercapacitors and Fabric Nanogenerators. *Adv Mater* 2016; 28(1): 98–105.

17. Joshi M and Butola BS. Application technologies for coating, lamination and finishing of technical textiles. In: *Advances in the dyeing and finishing of technical textiles*: Elsevier, 2013, p.355.

18. Pfann WG and Dorsi D. Magnetic Stirring Technique. *Rev Sci Instrum* 1957; 28(9): 720–720.

19. Aoki M, Ring TA and Haggerty JS. Analysis and modeling of the ultrasonic dispersion technique. *Adv Ceram Mater* 1987; 2(3A).

20. Sato K, Li J, Kamiya H, et al. Ultrasonic dispersion of TiO_2 nanoparticles in aqueous suspension. *J Am Ceram Soc* 2008; 91(8): 2481–2487.

21. Bilisik K and Syduzzaman M. Carbon nanotubes in carbon/epoxy multiscale textile preform composites: A review. *Polym Compos* 2021; 42(4): 1670–1697.

22. Schilde C, Mages-Sauter C, Kwade A, et al. Efficiency of different dispersing devices for dispersing nanosized silica and alumina. *Powder Technol* 2011; 207(1-3): 353–361.

23. VMA-GETZMANN GMBH. DISPERMAT® Bead Mills - Durable and economical Bead Mills, https://www.dispermat.com/bead-mills.html (accessed Aug 18, 2023).

24. Li Y, Zhang H, Bilotti E, et al. Optimization of three-roll mill parameters for in-situ exfoliation of graphene. MRS advances 2016.

25. Yasmin A, Abot JL and Daniel IM. Processing of clay/epoxy nanocomposites with a three-roll mill machine. *MRS Online Proceedings Library (OPL)* 2002; 740.

26. Ha J, Lee S and Park S. Effect of dispersion by three-roll milling on electrical properties and filler length of carbon nanotube composites. *Mater* 2019; 12(23): 3823.

27. Li C, Li J, Li Y, et al. Fabric defect detection in textile manufacturing: a survey of the state of the art. *Secur Commun Netw* 2021; 2021: 1–13.

28. Akovali G. *Advances in polymer coated textiles*: Smithers Rapra, 2012, p.178.

29. Chowdhary U. *Textile analysis, quality control & innovative uses*. Linus Learning, 2010, p.127.

30. Chong PTF. Colorimetry for textile applications. In: *Modern Textile Characterization Methods*. CRC Press, 2017, p.355.

31. Sabeenian RS, Paul E and Prakash C. Fabric defect detection and classification using modified VGG network. *J Text Inst* 2023; 114(7): 1032–1040.

32. Mo D and Wong WK. Fabric Defect Classification based on Deep Hashing Learning. *AATCC Journal of Research* 2021; 8(1_suppl): 191–201.

33. Zheng X, Zheng S, Kong Y, et al. Recent advances in surface defect inspection of industrial products using deep learning techniques. *Int J Adv Manuf Technol* 2021; 113: 35–58.

34. Runesson K, Skyttebol A and Lindgren LE. Nonlinear Finite Element Analysis and Applications to Welded Structures. In: Milne I, Ritchie RO and Karihaloo B (eds) *Comprehensive Structural Integrity*. Oxford: Pergamon, 2003, p.255.

35. Orellana J, Moreno-Villoslada I, Bose RK, et al. Self-healing polymer nanocomposite materials by Joule effect. *Polymers* 2021; 13(4): 649.

36. Prolongo SG, Moriche R, Del Rosario G, et al. Joule effect self-heating of epoxy composites reinforced with graphitic nanofillers. *Journal of Polymer Research* 2016; 23: 1–7.

37. Guo Z, Wang Y, Huang J, et al. Multi-functional and water-resistant conductive silver nanoparticle-decorated cotton textiles with excellent joule heating performances and human motion monitoring. *Cellulose* 2021; 28(11): 7483–7495.

38. Korzeniewska E, Duraj A, Krawczyk A, et al. Analysis of thermographic images of thin metal layers using grouping algorithms. *Przegląd Elektrotechniczny* 2016; 92(12): 73–76.

39. Korzeniewska E, Szczesny A, Krawczyk A, et al. Temperature distribution around thin electroconductive layers created on composite textile substrates. *Open Physics* 2018; 16(1): 37–41.

40. van Langenhove L. Smart textiles for protection: an overview. In: Chapman RA (ed) *Smart Textiles for Protection*: Woodhead Publishing, 2013, p.7.

41. Sánchez-Romate XF, González C, Jiménez-Suárez A, et al. Novel approach for damage detection in multiscale CNT-reinforced composites via wireless Joule heating monitoring. *Composites Sci Technol* 2022; 227: 109614.

42. Cortés A, Romate XFS, Jiménez-Suárez A, et al. 3D printed anti-icing and de-icing system based on CNT/GNP doped epoxy composites with self-curing and structural health monitoring capabilities. *Smart Mater Struct* 2020; 30(2): 025016.

43. Ruiz-Calleja T, Calderón-Villajos R, Bonet-Aracil M, et al. Thermoelectrical properties of graphene knife-coated cellulosic fabrics for defect monitoring in Joule-heated textiles. *J Ind Text* 2022; 51(5_suppl): 8884S-8905S.

44. Sakai M, Takabatake K, Tamura K, et al. Why do wet-particles adhere to a high-speed roll in a three-roll mill?. *Phys Fluids* 2019; 31(3): 033302.